NUMERICAL ESTIMATION OF ISOTHERMAL MOISTURE STORAGE AND TRANSPORT PROPERTIES

M. Islahuddin and H. Janssen
KU Leuven, Department of Civil Engineering, Building Physics Section
Kasteelpark Arenberg 40, 3000 Leuven, Belgium

ABSTRACT

Hygric properties of building materials have been examined experimentally as well as numerically. However, the standard experimental procedures for hygric property determination typically lead to incomplete data and require several weeks of repetitive experiments. Moreover, measurement of the storage and transport properties at intermediate saturations is complex. On the other hand, existing numerical approaches can estimate moisture transport property. However, these models require prior measurement data like moisture storage and saturated permeability. This study proposes an alternative faster approach by using pore-scale physics to estimate complete data of moisture storage and transport properties.

INTRODUCTION

The durability and sustainability of building envelopes as well as the health and comfort of building occupants are essential performance criteria for built constructions. And one key aspect to consider therein is the impact of moisture. Excessive interior humidity levels, for example, cause mould growth, which threatens occupant health and aesthetically harms the construction. Rebar corrosion is another example where pore water enables chloride infiltration and the resultant damage to reinforced concrete. Therefore the hygric behaviour of building components plays an essential role in determining performances, and its reliable assessment is hence crucial.

To quantify the response of built constructions towards moisture, storage and transport properties of building materials must be determined. The storage property can be experimentally identified by standard ad- and desorption techniques, such as desiccator tests for the hygroscopic regime and pressure plate tests for the saturated regime. The transport property can similarly be measured by cup and capillary absorption tests for the low and high moisture content range respectively. However, currently available measurement techniques are lacking for the mid-saturation range (where the relative humidity is between 97 and 99 %). Moreover, the capillary absorption test does neither give any accurate transport property for the overcapillary regime, due to the asymptotic second absorption phase resulting from the dissolution of entrapped air. Therefore, the existing experimental methods provide only incomplete characterisations of the storage and transport properties. Furthermore, these series of measurements typically require weeks to months for their full execution.

As an alternative approach, numerical estimations may offer a significantly more complete result in a considerably shorter time interval. Among these, pore network modelling is a promising approach. In this approach, the material's void space is represented as a discrete network of pore bodies and throats with simplified shapes. In addition to the pore space representation, relatively simple microlevel physical models are employed to simulate the relevant moisture behaviour, such as capillary condensation, surface adsorption, vapour diffusion, and liquid flow. The incorporation of this pore-scale method in this study is essential, as the macroscopic properties are of course dictated by the materials' microstructures (Bakke & Øren 1997). Therefore, a proper pore-scale-based physical model will best resemble the actual processes and material properties.

The pore network models commonly applied to estimate moisture transport of building materials suffer from the deficiency of the conceptual representation of pore space and the dependency on prior measurement data (Quenard & Sallee 1992; Descamps 1997; Carmeliet & Roels 2001). These models conceptually represent the complex pore spaces with regular lattices of pores and throats. The pore and throat shapes are idealized with cylindrical or angular cross-sections, with randomly generated sizes based on a premeasured pore size distribution. These conceptual pore network models oversimplify the complexity of the microstructures as pore connectivity, shape, and size have been identified to be significantly important (Parlar & Yortsos 1988; Vogel & Roth 2001; Jivkov et al. 2013). Therefore, they are inadequate both topologically and geometrically. On top of that, previously measured information on moisture storage was needed to generate a pore size distribution for artificial network models to simulate moisture permeability (Carmeliet & Roels 2001). In addition, the estimated unsaturated permeability curve had to be calibrated to the

measured permeabilities in low- and over-capillary ranges.

This study is therefore conducted to tackle the above mentioned flaws: the necessity of prior moisture storage and transport measurement, and the deficiency of the conceptual pore network model. To that end, the proposed approach employs a topological pore network model which is extracted from a voxelized computer tomography image to topologically and geometrically duplicate the real nature of the pore structure. The resulting network conserves the overall porosity, and the pore shapes, sizes, and connectivities. Hence, this topological network solves the deficiency of the existing conceptual pore network models. Subsequently, pore-scale physical storage and transport models are applied to the real-sized topological network to simulate the moisture-related physical processes. As a result, the moisture storage and transport properties can be simultaneously and reliably estimated, without any need for calibration.

In relation to Building Physics, this work allows a simultaneous estimation of complete moisture storage and transport properties. The approach is relatively faster and cheaper compared to existing experimental approaches.

PORE NETWORK MODEL

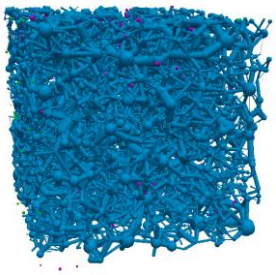

Figure 1: Pore network model of Berea sandstone extracted with maximal ball algorithm

The estimation of moisture storage and transport properties is performed via pore network modelling with its three components: a topological pore network as a pore space model, a percolation algorithm as an invasion procedure to define moisture storage, and a liquid flow/vapour diffusion model to simulate the moisture transport. The implementation of a percolation algorithm in an image-based pore network model defines the spatial moisture distribution and thus instantly and reliably estimates the moisture content. Subsequently, the moisture flow is simulated for the related moisture distribution to estimate the permeability. The simulation is performed under isothermal and equilibrium conditions. Moreover, the involved fluids are assumed to be incompressible and immiscible.

Pore space representation

In this simulation, a cubical sample of Berea sandstone is used as an exemplary material. Its pore space is digitized with micro-CT scanning and then a topologically equivalent network of pores and throats is extracted with a specific extraction method. Figure 1 shows the topological network of Berea sandstone extracted with the maximal ball algorithm (Dong & Blunt 2009). This extraction method is in principle based on the largest inscribed spheres in the void space to define pores and throats. Moreover, the algorithm also digitally determines the network's topological and geometrical properties. The topological features are related to the pore coordinates and connectivities, while the geometrical features describe the pore shapes and sizes.

Table 1:
Network properties

PROPERTY	VALUE
Sample side size [mm]	2.138
Porosity [-]	0.196
Average pore radius [μm]	15.36
Minimum pore radius [μm]	2.27
Maximum pore radius [μm]	70.25
Average throat radius [μm]	7.01
Minimum throat radius [μm]	0.54
Maximum throat radius [μm]	40.06
Number of pores [-]	6298
Number of throats [-]	12098

Table 1 lists some of the geometrical properties. Nearly the whole porosity contributes to storage and flow as the network is homogenous, as can be visually seen in Figure 1. Pore and throat radii are used to define entry capillary pressures which dictate moisture invasion and thus moisture storage. The radius distribution in Figure 2 confirms the homogeneity of the network and provides a better insight of the pore and throat sizes. For the flow properties, a dimensionless shape factor G (Mason & Morrow 1991) is derived from the image processing:

$$G = \frac{A}{p^2} \qquad (1)$$

with A = cross-sectional area [m^2], and p = perimeter [m], which are calculated from the voxelized CT image. This parameter is extracted to better represent the real shapes of pores and throats which are highly irregular. The pore network parameterization indeed assumes idealized cylindrical capillaries with a particular cross-sectional shape and other size parameters. The cross-sections are defined by the shape factor G to be either circular, square, or irregularly triangular. The analysis of the voxelized image also defines the size parameters: radius, length,

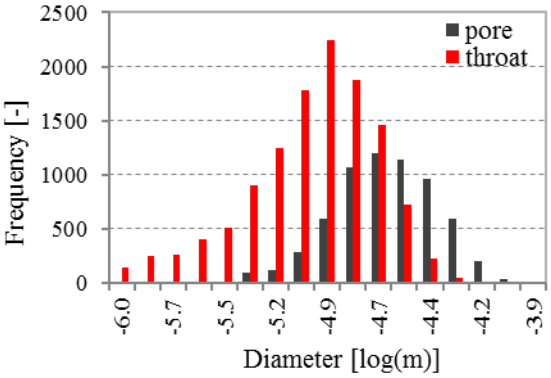

Figure 2: Pore size distribution of pore (black) and throat (red)

and volume. In this way, the network's topological and geometrical properties conserve the real nature of the pore space.

Storage

Moisture inside a porous medium is in two forms: vapour and water. The amount of vapour in moist air in a material is insignificant compared to the amount of water. Therefore, vapour in air is neglected in storage calculation. As a result, moisture content is mainly defined by the amount of water which is dictated by the invasion procedures of physical phenomena. Adsorption, imbibition, and desorption algorithms are developed to simulate desiccator, capillary absorption, and desorption tests, respectively. Ad- and desorption are required to analyse hysteresis, while imbibition is to yield the capillary moisture content. The resulting moisture distributions are used to calculate the moisture content from the amount of water in liquid islands after capillary condensation in pore and in adsorbed liquid films on the pore walls of dry pores.

The first algorithm is the adsorption, which refers to the invasion of moisture into a dry material by surface adsorption and capillary condensation of vapour contained in moist air. Capillary condensation occurs in a pore if the vapour pressure has reached its local saturation value. This pore saturation value is below the standard saturation value, as formulated in Kelvin's equation (Eq. 2):

$$p_v = p_{vsat} \exp\left(\frac{p_c}{\rho_l R_v T}\right) \qquad (2)$$

with p_v = vapour pressure [Pa], p_{vsat} = saturated vapour pressure [Pa], p_c = capillary pressure [Pa], ρ = water density [kg/m^3], R_v = vapour gas constant [J/kgK], and T = temperature [K].

To quantify this pore filling mechanism, and also the moisture transport process, capillary pressure is chosen to be the potential. This choice is preferred because capillary pressure has been investigated as the most preferred moisture potential due to its continuity and efficiency (Janssen 2014). In terms of this potential, capillary condensation occurs when the capillary pressure has reached the pore's entry capillary pressure. The Young-Laplace equation relates this entry capillary pressure to the pore radius, as formulated in Equation 3:

$$p_c = p_l - p_g = \frac{-2\sigma\cos(\theta)}{r} \qquad (3)$$

with p_c = capillary pressure [Pa], p_l = liquid pressure [Pa], p_g = gas pressure [Pa], σ = surface tension [N/m], θ = contact angle [-], and r = pore radius [m]. The contact angle is set to zero since water preferentially wets silicate materials. Note that Equation 2 and 3 imply a negative capillary pressure which differs from some other research areas.

Prior to condensation, at low capillary pressures, water vapour molecules are adsorbed to the pore walls due to van der Waals forces. A single layer of water molecules is formed during the first stage of this adsorption. As capillary pressure increases, multilayer structures of water molecules are assembled. It is assumed that the vapour pressure above this water film curvature is not affected by the decrease in pore radius. To assess the volume of both the mono- and multilayer cases, the statistical thickness of Bradley's equation (Eq. 4) is adopted. This formula has been reported to be relatively accurate in both the hygroscopic and over-hygroscopic regimes, and more accurate than other models (Badmann et al. 1981):

$$t_a(\varphi) = \left[K_1 + K_2 \ln\left(-\ln(\varphi)\right)\right] \cdot 10^{-10} \qquad (4)$$

with t_a = film thickness [m], and φ = relative humidity [-]. The same source also reported that the two constants for silicate materials are K_1 = 3.85 and K_2 = -1.89 .

Unlike adsorption, imbibition is a process where liquid water at a boundary side continuously infiltrates into the pore structure. The water front at one side of the material invades the adjacent pore having the smallest entry pressure. As a consequence, this invasion procedure forms a continuous water cluster.

Desorption refers to the evaporation, due to contact with air at a boundary, of water from an initially wet material. Pore water evaporates once the capillary pressure declines below the pore's entry capillary pressure. However, that is not the only requirement for phase change. The pore water has also to be connected to bulk air, allowing water vapour to diffuse and escape. This accessibility requirement may cause 'ink-bottle' effects, where water in big pores cannot evaporate due to blocking by smaller water-filled pores. As a result, evaporation in these big pores occurs later at smaller capillary pressures,

after the smaller pores. This makes the desorption moisture properties differ from that of adsorption/imbibition, thus forming an ad- and desorption curve cycle, which is known as hysteresis.

At the (over-)capillary moisture range, saturated and capillary moisture contents are different. This difference is due to air entrapment in which air is partially trapped in pores/throats (Janssen et al. 2015). To simulate this, an air entrapment procedure is integrated into the adsorption and imbibition algorithms. This introduces a new requirement for pore filling/invasion, since it has to have access to bulk air. The accessibility is required for air to escape, otherwise, air remains partially trapped. This entrapment is also due to the assumptions that the fluids are incompressible and immiscible.

Transport

For a spatial moisture distribution resulting from any of the invasion algorithms, a moisture flow is generated by applying a small pressure difference over two opposing boundaries. Moisture simultaneously flows in liquid and vapour form, since both phases coexist in unsaturated conditions. Vapour flows as Fickian diffusion in dry pores, while liquid flows as Hagen-Poiseuille flow in wet pores. For each two neighboring pores, the moisture flow is proportional to the product of the pressure difference and the moisture conductance:

$$q = g\ \Delta p_c \tag{5}$$

with q = moisture flow rate [kg/s], g = moisture conductance, and Δp_c = capillary pressure difference [Pa]. The moisture conductance between pore i and j is determined by the harmonic mean of pore and throat conductances:

$$g_{ij} = \left(\frac{1}{g_{l/v,i}} + \frac{1}{g_{l/v,t}} + \frac{1}{g_{l/v,j}} \right)^{-1} \tag{6}$$

with $g_{l/v,}$ = liquid (hydraulic)/vapour (diffusive) conductance, and subscript i, j, and t = pore i, j, and the connecting throat. The pore conductance is calculated based on the length from the pore center to the border.

The liquid conductances of wet pores/throats are calculated with the Hagen-Poiseuille equation:

$$g_l = \frac{c_G \rho_l r^4}{16 \mu_l L G} \tag{7}$$

with μ_l = dynamic viscosity of water liquid [kg/ms], c_G = a constant related to cross-sectional shape, G = shape factor [-], and L = pore/throat length [m]. The constant c_G are equal to 0.5, 0.5623, and 0.6 for circular, square, and triangular cross-sections, respectively (Patzek & Silin 2001; Øren et al. 1998).

The vapour conductances of dry pores/throats depend on the vapour pressure, as formulated in Equation 8:

$$g_v = \delta_v \frac{p_v}{\rho_l R_v T} \frac{A}{L} \tag{8}$$

with δ_v = vapour permeability of air [kg(msPa)$^{-1}$]. Due to Kelvin's law, which relates vapour pressure to capillary pressure, this diffusive conductance changes based on the capillary pressure. The other variables are constant, thus the diffusive conductance has an upper bound which is determined by the standard saturated vapour pressure.

In small pores though, vapour molecules may not normally diffuse as pore walls limit the molecules' random movements. The vapour molecules do not move based on their mean free path to collide with each other, instead they hit the pore walls more frequently. Therefore, the diffusive conductance is reduced, as quantified with the Knudsen formulation:

$$g_{v,K} = \frac{g_v}{1 + l_m / r} \tag{9}$$

with l_m = mean-free-path length [m].

Once all moisture conductances are calculated, a unit pressure difference is applied over two opposing sides, while the other sides are set to be impermeable. To calculate the flow through each throat, the pressure at each pore body has to be determined. This spatial pressure distribution in the network is determined by solving a linear system of equations derived from mass conservation at each pore body. For pore body i, the mass conservation is given by:

$$\sum_{j \in N_i} q_{ij} = 0 \tag{10}$$

with q_{ij} = conductance of throat connecting pore i and j, N_i = a set of neighboring pore indices of pore i. Having the spatial pressure distribution, the moisture flow can then be simulated.

To finally determine the network's effective moisture permeability, the total flow rate is calculated at the pores lying in a plane perpendicular to flow direction. The moisture permeability is then obtained by applying Darcy's law:

$$Q = \frac{A_n}{L_n} k\ \Delta p_c \tag{11}$$

with Q = total macroscopic flow rate [kg/s], A_n = network's cross-sectional area [m^2], L_n = network's length [m], and k = effective moisture permeability [kg(msPa)$^{-1}$].

RESULTS

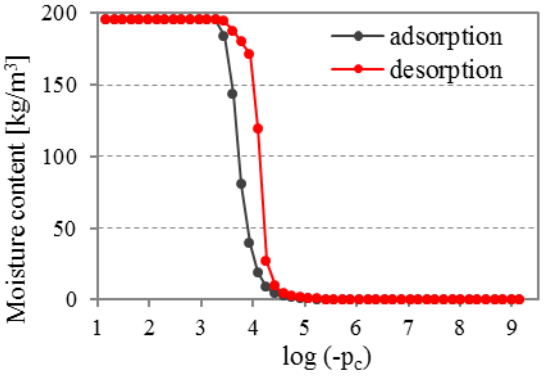

Figure 3: Moisture retention curves of adsorption (black) and desorption (red)

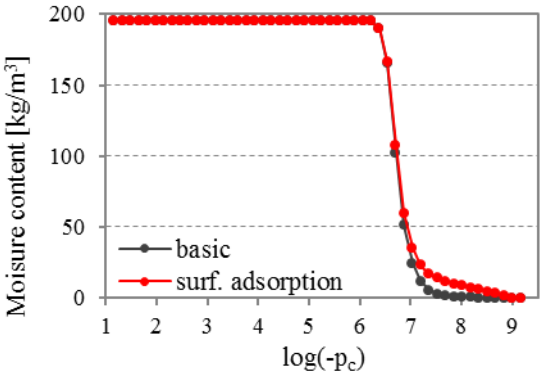

Figure 4: Moisture retention curves of scaled-down Berea network with (red) and without (black) surface adsorption

Storage

Figure 3 shows the numerical estimations of moisture retention curves of both adsorption and desorption. In the adsorption curve, the maximum value is the saturated moisture content, as air entrapment is not incorporated in this percolation algorithm. Furthermore, the existence of a single steep slope confirms that the Berea sample consists only of coarse pores and operates in the capillary regime governed by capillary condensation. Moreover, the zero moisture content in the hygroscopic regime in Figure 3 and the minimum pore and throat sizes in Table 1 indicate that Berea sandstone is a non-hygroscopic material. This implies that surface adsorption is insignificant for the overall moisture storage. Note that this conclusion is limited to the Berea network. However, standard building materials are generally hygroscopic in which surface adsorption may play significant roles. Therefore, the Berea network is scaled down 1000 times to allow the analysis of surface adsorption.

The scaled-down process yields a hygroscopic network in which moisture content increases in the hygroscopic region, as shown in Figure 4. The figure displays moisture retention curves with and without surface adsorption. At low capillary pressures, both curves differ quite significantly. The moisture content with surface adsorption is higher than that of without surface adsorption. Therefore, the increment of moisture content in hygroscopic region is attributed to the volume of the adsorbed water films.

The volumetric significance of the adsorbed water films in the scaled-down Berea network is due to two factors. The first one is that the surface area of micropores is larger than that of macropores. This results in more water molecules adsorbed on the surface walls. However, this effect is macroscopically significant if the microporosity is substantial in comparison to the macroporosity. Therefore, the second factor is because the volume of water films is significant compared to the total volume of water islands in the whole network.

The conclusion that surface adsorption considerably affects the moisture content of hygroscopic materials suggests that the microporosity in multipore systems of typical building materials is important and thus cannot be neglected.

The desorption curve (Fig. 3) does not coincide with the adsorption curve. The first desorption of the pores need not occur at the last-filled pore, due to the accessibility requirement. Therefore, as the capillary pressure decreases, desorption starts from the boundary pores that are exposed to bulk air. Water in these pores evaporates sequentially from big to small, and from boundary to inner pores. Since pores are connected to throats, and pore sizes are commonly larger than throat sizes, pore water evaporates at much smaller capillary pressures than would be expected. The moisture content differences of adsorption and desorption are quite large, up to 145 kg/m^3 at about -10^4 Pa. As throats become dry, massive evaporation in pores follows. This explains the very steep drop in the over-hygroscopic regime. The non-hygroscopicity of this material dictates no more drop in hygroscopic region.

The incorporation of air entrapment into the percolation algorithm significantly affects the moisture storage as shown in Figure 5. This yields a reduced maximum moisture content which is called the capillary moisture content. However, the maximum moisture content of adsorption percolation is unrealistically reduced. Moreover, the air entrapment also occurs in the beginning of capillary regime, thus decreasing the moisture content considerably. This decline in over- and capillary regimes is because capillary condensation first occurs in small throats and pores, thus trapping air in many of the larger pores and throats.

The concept of capillary moisture content is instead attributed to a capillary absorption measurement, in which moisture originates from the invasion of water at boundaries. Therefore, air entrapment is well

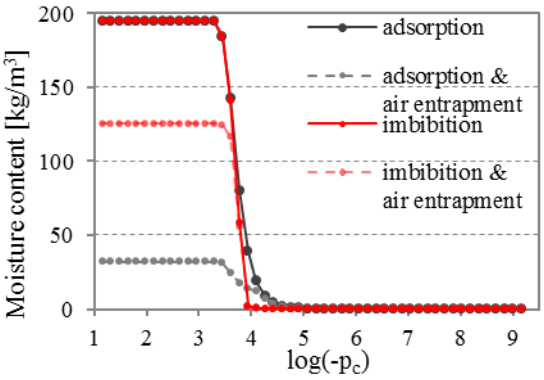

Figure 5: Air entrapment (dashed lines) effect to moisture retention curves of adsorption (black) and imbibition (red) simulations

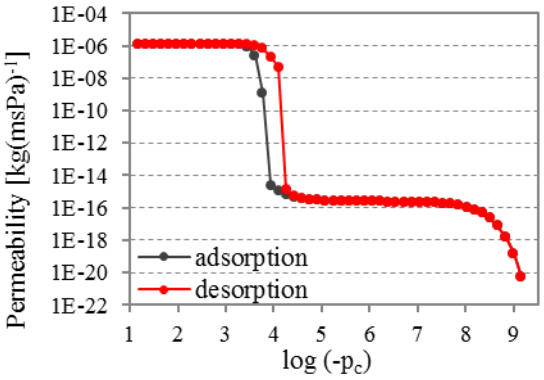

Figure 6: Permeability curves of adsorption (black) and desorption (red) simulations, as a function of log capillary pressure

suited to imbibition percolation, rather than to adsorption percolation, to produce the capillary moisture content. Figure 5 confirms this hypothesis where the capillary moisture content of imbibition percolation is a fair amount smaller than the saturated one. This is because the invasion procedure always yields a spatially continuous water cluster which naturally limits the amount of trapped air.

The adsorption and imbibition curves differ in the low saturation range (Fig. 5). In imbibition, the moisture content starts rising when the water front invades the smallest neighboring boundary pores. These pores are more likely to have bigger entry capillary pressures than the smallest entry capillary pressure. Therefore, the moisture content of imbibition is smaller than that of adsorption.

Transport

At low capillary pressures (or low relative humidities), moisture is only transferred via vapour diffusion. The permeability increment in this region (between -10^{-9} and -10^{-8} Pa) , as shown in Figure 6, is merely attributed to the rise of vapour pressure, see Equation 7, as capillary condensation is not occurring yet. In contrast to vapour diffusion, saturated permeability is defined by dominant liquid flow having a significantly higher permeability value.

The transition zone in the adsorption permeability curve consists of a unique steep rise due to the single pore system with coarse pores. In the beginning of this capillary region, condensation in relatively small pores forms liquid islands which enhance the moisture transfer due to the combination of vapour and liquid transfers. Moreover, as capillary pressure increases, liquid islands start spanning the opposing sides in which moisture is transferred solely by liquid form. This moment induces a substantial rise in the permeability curve. Further capillary condensation in the largest pores enlarges these islands or creates new spanning liquid islands.

In the desorption permeability curve, as capillary pressure decreases, the maximum permeability value can be maintained until the first desorption occurs.

The permeability drops are insignificant in this over-hygroscopic region since the spanning liquid island clusters still exist. As a result, the permeability differences between adsorption and desorption curves are quite large. In Figure 6, at capillary pressure -10^{4} Pa, the differences are comparable to the difference between liquid and vapour permeabilities. As desorption continues, the spanning liquid islands disappear and thus the permeability drops considerably.

The presentation of permeability with respect to moisture content is shown in Figure 7 with a finer grid. The ad- and desorption curve cycle in the figure exposes the importance of spatial water-island distribution to moisture flow. At the same moisture content, the permeabilities of ad- and desorption may differ due to the difference in spatial distribution of water liquid in the pore network. The discrepancy supports the claim that pore topology (connectivity) and geometry (size) are very important in dictating the pore-scale physical phenomena. This permeability difference disagrees with the common assumption in

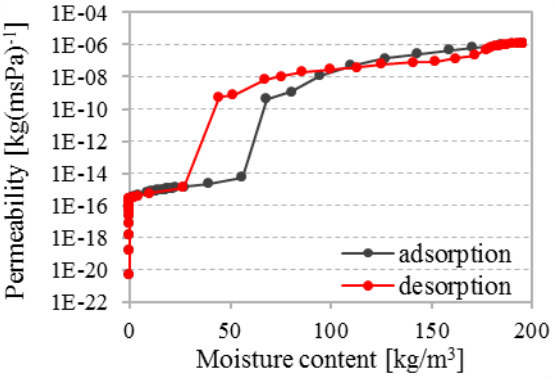

Figure 7: Permeability curves of adsorption (black) and desorption (red) simulations, as a function of moisture content

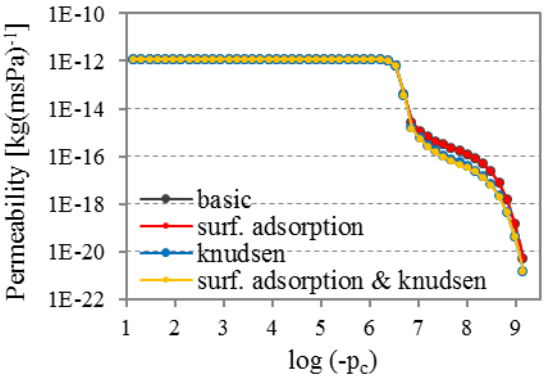

Figure 8: Permeability curves of the scaled-down Berea network without both surface adsorption and Knudsen (black), with surface adsorption (red), with Knudsen (blue), and with both surface adsorption and Knudsen (yellow)

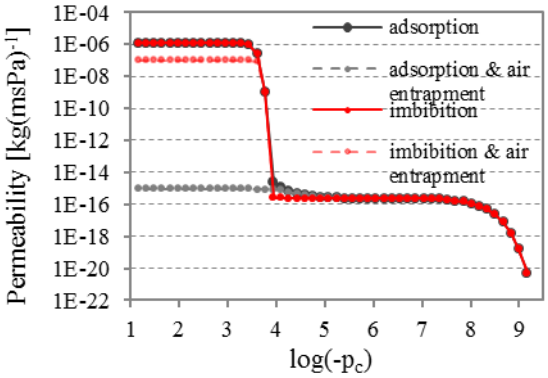

Figure 9: Air entrapment (dashed lines) effect to permeability curves of adsorption (black) and imbibition (red) simulations

macroscopic hygric-property analysis which assumes a unique permeability value at the same moisture content.

In the normal Berea network, the effect of Knudsen diffusion on the network's moisture permeability is negligible. This is because the pore sizes are bigger than the mean free path of the vapour molecules. However, in the scaled-down Berea network, the pore sizes are smaller than the mean free path. Therefore, the Knudsen diffusion plays an important role. The collision of vapour molecules with the pore walls decreases the random movements and collisions, thus reducing the overall moisture permeability.

The quantitative effect of Knudsen and surface adsorption is confirmed in Figure 8. The figure shows that the permeability curves with and without Knudsen diffusion appreciably differ. This difference mainly occurs in the hygroscopic regime and becomes less in the capillary regime due to condensation.

The integration of surface adsorption slightly decreases the permeability due to the constriction of the pore's cross-section. This constriction strengthens the Knudsen effect as the water film thickness is quite notable in decreasing pore radii. As a result, the vapour molecules more frequently collide with the pore wall, thus decreasing the diffusion process. However, the effect of surface adsorption itself is negligible in the absence of Knudsen diffusion.

Figure 9 shows the impact of entrapped air on the permeabilities. The permeability corresponding to the adsorption capillary moisture content is remarkably smaller than that of the saturated one. This is because the highly reduced maximum moisture content does not reach the critical value for which a spanning liquid islands' cluster exists. Therefore, vapour-filled pores hinder the relatively fast flow in liquid islands, resulting in small effective permeabilities.

Similar to the moisture storage, the integration of air entrapment into imbibition algorithm yields reasonable permeability results (Fig. 9). The maximum permeability that corresponds to the capillary moisture content is realistically reduced compared to the saturated permeability. This is due to the appropriate invasion percolation that mimics the imbibition process in a better way.

LIMITATIONS

The presented approach is applied to a pore network model that inherits the limitations from the corresponding image processing and network extraction algorithm. Different extraction methods result in different topological and geometrical properties. They differ from the adopted approach in the distinction between pores and throats, and in the extraction of pore and throat sizes.

The maximal ball algorithm that is used to extract Berea network model (Dong 2007), for example, has to adjust the throat radii to guarantee continuity of predicted properties. Moreover, the author recommends to compare this property with the result from mercury intrusion experiment and NMR to attenuate the uncertainties inherited from image processing.

The physical model is also limited to the following assumptions: isothermal and equilibrium conditions, and incompressible and immiscible fluids. An advancement with respect to the assumptions may give slightly different results and allow to analyse more phenomena. For instance, a dynamic model would permit analysis of dynamic effects, while implementation of air compressibility may reduce the entrapped air. However, the proposed method has already included the most significant features for a reliable first assessment.

Another limitation of this study is the unavailability of measurement data for validation purposes. The full measurement of moisture storage and transport properties and the complete characterization of building materials' pore structures are still

problematic and will be dealt with in our future projects. In this study, we focus only on the simulation method.

CONCLUSION

This paper has presented an approach for numerically estimating the moisture storage and transport properties of a porous building material.

The permeability estimation is highly dependent to the given spatial moisture distribution, not only to the moisture content as commonly assumed in experiments. As already shown in the simulation, the most important enhancement in permeability is due to the existence of spanning liquid islands.

The incorporation of the air entrapment into the system significantly affects the results. Both the storage and the transport properties are reduced correspondingly.

For hygroscopic materials, surface adsorption plays an important role in both moisture storage and transport. However, the contribution to transport is less significant than that of storage. This is because the effect of surface adsorption is assumed to be limited to the pore constriction which decreases diffusion process.

The capability of this approach to estimate both moisture storage and transport directly eliminates the requirement of existing pore network models (Carmeliet & Roels 2001; Quenard & Sallee 1992; Satik & Yortsos 1995) to be supplied by measured storage and transport properties. In return, an extracted pore network model is needed. To get this pore network, imaging and extraction processes have to be performed. However, the resulting network model is reusable and allows a reliable and much faster estimation process. Therefore, this estimation model is a promising alternative to experimental measurement for hygric-property evaluation and design.

ACKNOWLEDGEMENT

This research project is supported by The Research Foundation – Flanders (FWO) through Odysseusprogramme.

REFERENCES

Badmann, R., Stockhausen, N. & Setzer, M.J., 1981. The statistical thickness and the chemical potential of adsorbed water films. *Journal of Colloid and Interface Science*, 82(2), pp.534–542.

Bakke, S. & Øren, P.-E., 1997. 3-D Pore-Scale Modelling of Sandstones and Flow Simulations in the Pore Networks. *SPE Journal*, 2(2).

Carmeliet, J. & Roels, S., 2001. Determination of the isothermal moisture transport properties of porous building materials. *Journal of Building Physics*, 24(3), pp.183–210.

Descamps, F., 1997. *Continuum and discrete modelling of isothermal water and air flow in porous media*. KU Leuven, Belgium.

Dong, H., 2007. *Micro-CT imaging and pore network extraction*. Imperial College London.

Dong, H. & Blunt, M.J., 2009. Pore-network extraction from micro-computerized-tomography images. *Physical Review E*, 80(3), p.036307.

Janssen, H., 2014. Simulation efficiency and accuracy of different moisture transfer potentials. *Journal of Building Performance Simulation*, 7(5), pp.379–389.

Janssen, H., Vereecken, E. & Holúbek, M., 2015. A Confrontation of Two Concepts for the Description of the Over-capillary Moisture Range: Air Entrapment versus Low Capillarity. *Energy Procedia*, 78, pp.1490–1494.

Jivkov, A.P. et al., 2013. A novel architecture for pore network modelling with applications to permeability of porous media. *Journal of Hydrology*, 486, pp.246–258.

Mason, G. & Morrow, N.R., 1991. Capillary behavior of a perfectly wetting liquid in irregular triangular tubes. *Journal of Colloid and Interface Science*, 141(1), pp.262–274.

Øren, P.E., Bakke, S. & Arntzen, O.J., 1998. Extending Predictive Capabilities to Network Models. *Proceedings of SPE Annual Technical Conference and Exhibition*.

Parlar, M. & Yortsos, Y.., 1988. Percolation theory of vapor adsorption—desorption processes in porous materials. *Journal of Colloid and Interface Science*, 124(1), pp.162–176.

Patzek, T.W. & Silin, D.B., 2001. Shape Factor Correlations of Hydraulic Conductance in Noncircular Capillaries. *Journal of colloid and interface science*, 236, pp.295–304.

Quenard, D. & Sallee, H., 1992. Water vapour adsorption and transfer in cement-based materials: a network simulation. *Materials and Structures*, 25, pp.515–522.

Satik, C. & Yortsos, Y.C., 1995. A pore network model for adsorption in porous media. In *Proceedings Twentieth Workshop on Geothermal Reservoir Engineering*. Stanford, California.

Vogel, H.J. & Roth, K., 2001. Quantitative morphology and network representation of soil pore structure. *Advances in Water Resources*, 24, pp.233–242.